Zero-Field ^{53}Cr Nuclear Magnetic Resonance in Ferromagnetic CrI_3: Renormalized Spin-Wave and Green's-Function Analysis*

ALBERT NARATH
Sandia Laboratory, Albuquerque, New Mexico
(Received 15 June 1965)

The zero-field ^{53}Cr nuclear magnetic resonance (NMR) has been studied in ferromagnetic CrI_3 in the temperature range 1.6–27.5°K. The observed spectrum consists of a quadrupole triplet ($h^{-1}e^2qQ=0.744 \pm 0.005$ Mc/sec) arising from nuclei within the ferromagnetic domains, and a broad absorption at lower frequencies due to nuclei in domain walls. The difference between the domain and wall frequencies follows the relation $\Delta\nu$ (Mc/sec)$=0.8(\pm 0.1)+0.248(\pm 0.005)T$ over the entire range of our experiments, where T is the temperature in °K. The temperature dependence of the domain magnetization, as derived from the resonance data, is in excellent agreement with predictions of a renormalized spin-wave model using values for the intralayer and interlayer exchange constants of $J_T/k_B=13.5\pm 0.5$°K and $J_L/k_B=1.72\pm 0.20$°K, respectively, and a published value for the uniaxial anisotropy constant. The extrapolated 0°K zero-field $\frac{1}{2}\leftrightarrow -\frac{1}{2}$ ^{53}Cr NMR frequency is $\nu(0)=49.393$ Mc/sec. The results of the spin-wave analysis are supported by calculations of the Curie temperatures for $CrBr_3$ and CrI_3 using the random-phase Green's-function method, based on the spin-wave-derived exchange constants. The calculated values of 33.6°K for $CrBr_3$ and 68.2°K for CrI_3 are in excellent agreement with reported experimental ordering temperatures of 32.5° and 68°K, respectively.

I. INTRODUCTION

In recent years considerable attention has been focused on the magnetic properties of the anhydrous chromium (III) halides CrX_3 (X = Cl, Br, I). These compounds crystallize in sandwich structures in which hexagonal sheets of Cr^{3+} ions are separated from adjacent layers by two close-packed layers of halogen ions. At low temperatures the crystal structures of $CrCl_3$ and $CrBr_3$ are isomorphous.[1,2] The unit cell has rhombohedral symmetry (space group $R\bar{3}$). The detailed structure of CrI_3, however, is somewhat uncertain.[1,3] It is either identical to that of $CrCl_3$ and $CrBr_3$ or differs at most in the stacking arrangement of the chromium-halogen sandwiches. As a result of the large separation between Cr^{3+} layers, the interlayer exchange forces are considerably weaker than those which couple intralayer spin pairs. The intralayer interaction is ferromagnetic. The net interlayer interaction is antiferromagnetic[4] in the chloride ($T_N=16.8$°K)[5] and ferromagnetic[6] in the bromide ($T_C=32.5$°K).[7] The continuing interest in these compounds is due in large part to the success with which many experimental observations have been correlated with detailed theoretical calculations. In particular, comparisons of ^{53}Cr nuclear magnetic resonance measurements of the low-temperature sublattice magnetizations of $CrCl_3$[8] and $CrBr_3$[9] with predictions of a renormalized spin-wave model have led to an accurate determination of the important exchange parameters. For example, the ratio of intralayer to interlayer exchange energies at 0°K was found to be 426 in $CrCl_3$ and 25 in $CrBr_3$.

The bulk magnetic properties of CrI_3 were first investigated by Hansen and Griffel.[10] They obtained a large, positive paramagnetic Curie temperature ($\theta\simeq 70$°K) from susceptibility measurements on polycrystalline specimens in the range 20–375°K. A pronounced remanent magnetization was observed at 4.2°K. The presence of a spontaneous ferromagnetic moment in zero field was subsequently confirmed by measurements of the field-dependence of the ^{53}Cr NMR intensity,[11] as well as by studies of the magneto-optical properties[12] of CrI_3. A ferromagnetic Curie temperature of 68°K has been inferred[12] on the basis of bulk magnetization measurements. The 4.2°K saturation moment is $3.10\mu_B$. Ferromagnetic resonance experiments[12] have given $g_{\parallel}=2.07$ and have established that the easy direction of magnetization coincides with the hexagonal c axis (i.e., normal to the two-dimensional Cr^{3+} arrays). The magnetic anisotropy has uniaxial symmetry with $H_A=28.6$ kOe at 1.5°K.

The purpose of the present paper is to report on a zero-field investigation of the ^{53}Cr NMR in ferromagnetic CrI_3, and to relate the present results to our earlier work on $CrCl_3$ and $CrBr_3$. The observed temperature dependence of the CrI_3 sublattice magnetization has been analyzed by means of the renormalized spin-wave model developed previously[9] for $CrBr_3$. The validity of the exchange constants obtained from a fit of spin-wave theory to experiment has been verified by a random-

* This work was supported by the U. S. Atomic Energy Commission.
[1] B. Morosin and A. Narath, J. Chem. Phys. **40**, 1958 (1964).
[2] A. Braekken, Kgl. Norske Videnskab. Selskabs Forh. **5**, No. 11 (1932).
[3] L. L. Handy and N. W. Gregory, J. Am. Chem. Soc. **74**, 891 (1952).
[4] J. W. Cable, M. K. Wilkinson, and E. O. Wollan, J. Phys. Chem. Solids **19**, 29 (1961).
[5] W. N. Hansen and M. Griffel, J. Chem. Phys. **28**, 902 (1958).
[6] J. F. Dillon, Jr., J. Phys. Soc. Japan **19**, 1662 (1964).
[7] From specific-heat measurements by L. D. Jennings and W. N. Hansen, Phys. Rev. **139**, A1693 (1965).
[8] A. Narath and H. L. Davis, Phys. Rev. **137**, A163 (1965).
[9] H. L. Davis and A. Narath, Phys. Rev. **134**, A433 (1964).
[10] W. N. Hansen and M. Griffel, J. Chem. Phys. **30**, 913 (1959); W. N. Hansen, J. Appl. Phys. Suppl. **30**, 304S (1959).
[11] A. Narath, Bull. Am. Phys. Soc. **7**, 481 (1962).
[12] J. F. Dillon, Jr. and C. E. Olson, J. Appl. Phys. **36**, 1259 (1965).

phase Green's function calculation of the Curie temperature. The experimental techniques and the results of the NMR measurements are presented in Sec. II. The spin-wave analysis of our CrI_3 data is carried out in Sec. III. The Green's function method is applied to the calculation of T_C for CrI_3 and $CrBr_3$ in Sec. IV. The results of our investigation are summarized and discussed in Sec. V.

II. EXPERIMENTAL DETAILS

A. Techniques

The samples of CrI_3 used in this investigation consisted of polycrystalline aggregates which were obtained by allowing chromium metal to react with iodine at elevated temperatures. Measurements were made on two different sample preparations. The first was prepared by J. E. Hesse following the method of Handy and Gregory.[13] Although pure CrI_3 is reported to be extremely stable[13] at room temperature, this specimen decomposed gradually over a period of approximately one year. The decomposition apparently involved chemical reduction to the diiodide under the influence of moisture or atmospheric oxygen. This process appears to be accelerated by the presence of Cr^{2+} impurities. Our final measurements utilized a sample[12] of CrI_3 which was kindly provided us by Dr. C. E. Olson. The measured frequencies of the ^{53}Cr NMR in this sample were identical to those observed in our original specimen of CrI_3 at temperatures where a comparison was possible.

The zero-field ^{53}Cr resonances were observed with a push-pull FM marginal oscillator[14] followed by synchronous detection. The CrI_3 sample was contained in a narrow-tail glass Dewar whose sample tip was platinized but did not have the normal liquid-nitrogen radiation shield. The oscillator coil surrounded the outside of the tip. Filling factors of about 25% were realized with this arrangement.

Variable temperatures were achieved by controlling the pressure over baths of liquid helium, hydrogen, and neon. Temperature measurements were based on the appropriate vapor-pressure scales.[15] Hydrostatic head corrections were applied where necessary. The vapor-pressure measurements were checked against a calibrated germanium resistance thermometer[9] in the helium and hydrogen ranges, and against a calibrated platinum-resistance thermometer in the neon range. Differences between the vapor pressure and resistance measurements never exceeded 0.01, 0.02, and 0.04°K for the three cryogenic baths, respectively.

B. Results

The 0°K magnitude of the ^{53}Cr hyperfine field in CrI_3 was expected to be smaller than those observed in $CrCl_3$ and $CrBr_3$. This follows because overlap and covalency effects are expected to be larger for the more polarizable I^- ligands than the other halides. The resulting increase in the delocalization of the magnetic electrons should decrease the magnitude of the negative core polarization field at the chromium nucleus. In addition, orbital effects are also expected to be more important in the iodide. Since the internal field is negative in these compounds,[8,16] the orbital interaction in $CrI_3(g_{\parallel}>2)$ should produce an additional decrease in the total hyperfine field. For these reasons a search for the zero-field ^{53}Cr resonances was carried out at 4.0°K in the frequency range below 58 Mc/sec. The ^{53}Cr nuclear resonance spectrum was found to consist of three narrow, equally spaced absorption lines and a much broader single line at a lower frequency. The qualitative characteristics of this spectrum are strikingly similar to those reported by Gossard *et al.*[17] for ferromagnetic $CrBr_3$. The triplet pattern is evidently due to quadrupole splitting of the ^{53}Cr resonance ($I=\frac{3}{2}$) arising from nuclei situated within the ferromagnetic domains. The broader resonance is associated with nuclear-resonance processes in domain walls. Because of the variation of the direction of magnetization across the width of the wall, the angle between the hyperfine field and the principal electric-field-gradient (EFG) axis is position dependent. As a consequence, the quadrupole splitting is not resolved in the wall resonance. The 4.0°K width of the wall resonance is approximately 400 kc/sec, while the width of each triplet component is approximately 30 kc/sec. The spacing between the outer satellites of the triplet is 744 ± 5 kc/sec. Since the internal magnetic field direction at the ^{53}Cr nucleus coincides with the major principal EFG axis, the splitting corresponds to a quadrupole coupling constant $h^{-1}e^2qQ=0.744$ Mc/sec.

The integrated intensity of the domain resonances is smaller than that observed in $CrBr_3$ using the same apparatus. The reduction is consistent with the larger magnetic anisotropy of CrI_3[12] compared to $CrBr_3$[18] because of the H_A^{-1} dependence of the domain-rotation enhancement mechanism.[19] As in the case of $CrBr_3$, the wall resonance has a much greater integrated intensity than the domain resonance. This observation is in accord with the stronger enhancement predicted[20] for the wall absorption process.

The temperature dependences of the domain and wall resonances were measured in the range 1.6–27.5°K. The results are shown in Fig. 1. The separation between the components of the quadrupole triplet was found to be

[13] L. L. Handy and N. W. Gregory, J. Am. Chem. Soc. **72**, 5049 (1950).

[14] R. G. Shulman, Phys. Rev. **121**, 125 (1961).

[15] The liquid neon scale was taken from E. R. Grilly, Cryogenics **2**, 226 (1962).

[16] A. C. Gossard, V. Jaccarino, and J. P. Remeika, Phys. Rev. Letters **7**, 122 (1961).

[17] A. C. Gossard, V. Jaccarino, and J. P. Remeika, J. Appl. Phys. Suppl. **33**, 1187 (1962).

[18] J. F. Dillon, Jr., J. Appl. Phys. Suppl. **33**, 1191 (1962).

[19] A. C. Gossard and A. M. Portis, Phys. Rev. Letters **3**, 164 (1959).

[20] A. M. Portis and A. C. Gossard, J. Appl. Phys. Suppl. **31**, 205S (1960).

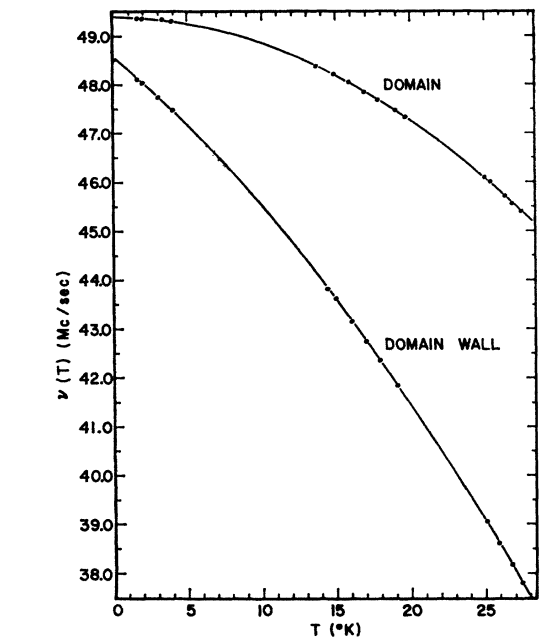

FIG. 1. Plot of the domain and domain-wall ^{53}Cr NMR in ferromagnetic CrI_3 as a function of temperature. For the domain resonance only the central ($\frac{1}{2}\leftrightarrow-\frac{1}{2}$) transition frequency is shown. The solid lines are smooth fits to the data.

independent of temperature in this range. The wall resonance frequency is seen to decrease much more rapidly with increasing temperature than is the case for the domain resonance. The difference between the two frequencies (measured relative to the central component of the triplet) follows within our experimental uncertainty the relation

$$\nu(T)_{\text{domain}}-\nu(T)_{\text{wall}}=0.8(\pm0.1)+0.248(\pm0.005)T(\text{Mc/sec}). \quad (2.1)$$

A similar expression has been reported by Gossard *et al.*[17] for $CrBr_3$:

$$\nu(T)_{\text{domain}}-\nu(T)_{\text{wall}}=1.07+0.289T(\text{Mc/sec}). \quad (2.2)$$

The relatively large uncertainty in the constant term of (2.1) is related to the uncertainty in defining the exact center of the wall signal. Similarly, the largest source of error in our temperature dependence measurements was introduced by changes in the observed line shapes with increasing temperature. These changes gave rise to estimated maximum errors in our experimental results of approximately ±15 kc/sec for the domain frequencies and ±200 kc/sec for the wall frequencies.

III. SUBLATTICE MAGNETIZATION ANALYSIS

In the following we make the usual assumption that the zero-field NMR frequencies are directly proportional to the thermal average values of the sublattice magnetization. This assumption is only valid if the hyperfine coupling constant is independent of temperature. The temperatures in our experiments were sufficiently low that thermal expansion effects were probably quite small. Thus, the above assumption appears to be well justified.

In order to make the comparison of experiment with theory tractable we adopt the same lattice model (Fig. 2) used successfully in the $CrCl_3$, $CrBr_3$ studies. This model is obtained by moving the Cr^{3+} sheets relative to each other until a superposition of all Cr^{3+} lattice positions along the c axis is attained. In this idealized structure the interlayer interaction can be described by a single exchange parameter, J_L. The intralayer parameter is denoted by J_T. Since CrI_3 is ferromagnetic, we assume that $J_L>0$ and $J_T>0$. The spin-wave spectrum for this model is expected to be a good approximation to the real spectrum provided that the interlayer interaction is much smaller than the intralayer interaction. This condition is satisfied in the chloride and bromide, and is expected to hold also in the iodide.

A. Domain Magnetization

The effects of exchange and anisotropy on the lowest orbital state of the Cr^{3+} ions can be described by the zero-field Hamiltonian

$$\mathcal{H}=-\sum_{ii',pp'}J_{ii',pp'}\mathbf{S}_{ip}\cdot\mathbf{S}_{i'p'}-D\sum_{i,p}(S_{ip}^z)^2, \quad (3.1)$$

where i labels the cell and $p(=1,2)$ labels the two nonequivalent sites in the magnetic unit cell of Fig. 2.

At sufficiently low temperatures it is possible to write the anisotropic terms as

$$D(S_{ip}^z)^2=g\mu_B H_A(T)S_{ip}^z. \quad (3.2)$$

The effective anisotropy field, $H_A(T)$ has the 0°K value $H_A(0)=2DS/g\mu_B$, where $S=\frac{3}{2}$ for Cr^{3+}. This definition of $H_A(T)$ is exact only in the classical limit. Its use in the present case is consistent, however, with the Green's-function decoupling scheme (4.6) employed in Sec. IV.

The approximate eigenvalues of (3.1), (3.2) have been discussed in connection with our previous work[8,9] on $CrCl_3$ and $CrBr_3$, and we shall outline their derivation only briefly. Starting with the Hamiltonian

$$\mathcal{H}=-J_T\sum_{ii',pp'}\mathbf{S}_{ip}\cdot\mathbf{S}_{i'p'}-J_L\sum_{ii',p}\mathbf{S}_{ip}\cdot\mathbf{S}_{i'p}-g\mu_B H_A(T)\sum_{i,p}S_{ip}^z, \quad (3.3)$$

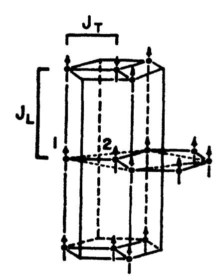

FIG. 2. Structure model for CrI_3 on which the calculations described in the text are based. The numbered positions refer to the two nonequivalent lattice sites.

we introduce boson operators according to[21-23]

$$S_{ip}^{+}=(2S)^{1/2}[1-(2S)^{-1}a_{ip}^{\dagger}a_{ip}]a_{ip},$$
$$S_{ip}^{-}=(2S)^{1/2}a_{ip}^{\dagger},\tag{3.4}$$
$$S_{ip}^{z}=S-a_{ip}^{\dagger}a_{ip},$$

and obtain

$$\mathcal{H}=\mathcal{H}_0+\mathcal{H}_1,\tag{3.5}$$

where

$$\mathcal{H}_0=E_0-2J_TS\sum_{ii',pp'}a_{ip}^{\dagger}a_{i'p'}-2J_LS\sum_{ii',p}a_{ip}^{\dagger}a_{i'p}+[2J_Tz_TS+2J_Lz_LS+g\mu_BH_A(T)]\times\sum_{i,p}a_{ip}^{\dagger}a_{ip}\tag{3.6}$$

$$E_0=-N[2J_Tz_TS^2+2J_Lz_LS^2+2g\mu_BSH_A(T)],$$

and

$$\mathcal{H}_1=J_T\sum_{ii',pp'}[a_{ip}^{\dagger}a_{ip}a_{ip}a_{i'p'}^{\dagger}-a_{ip}^{\dagger}a_{ip}a_{i'p'}^{\dagger}a_{i'p'}]+J_L\sum_{ii',p}[a_{ip}^{\dagger}a_{ip}a_{ip}a_{i'p}^{\dagger}-a_{ip}^{\dagger}a_{ip}a_{i'p}^{\dagger}a_{i'p}].\tag{3.7}$$

The sums in (3.3), (3.6), and (3.7) whose terms connect different lattice points include only those pairs which are coupled by an appropriate exchange constant. The number of neighbors which are exchange coupled to a given spin by J_T and J_L are denoted by $z_T(=3)$ and $z_L(=2)$, respectively. The quadratic part ($\mathcal{H}_0$) of $\mathcal{H}$ gives the linearized spin-wave states while the quartic part ($\mathcal{H}_1$) gives rise to interactions between these states. The effect of $\mathcal{H}_1$ vanishes as $T\rightarrow 0$. Furthermore, at sufficiently low temperatures the corrections to the spin-wave energies are proportional to the mean excitation energy,[24] and are thus quite small. For this reason it is sufficient to consider only those contributions of $\mathcal{H}_1$ which are diagonal in the diagonal representation of $\mathcal{H}_0$. The transformation which diagonalizes $\mathcal{H}_0$ was given in Ref. 9. We obtain

$$\mathcal{H}_0=E_0+\sum_{\mathbf{k},s}\omega_{\mathbf{k}s}n_{\mathbf{k}s},\quad n_{\mathbf{k}s}=0,1,2,\cdots$$
$$\omega_{\mathbf{k}s}=2J_Tz_TS[1-(-1)^s|\gamma_{(T)\mathbf{k}}|]+2J_Lz_LS[1-\gamma_{(L)\mathbf{k}}]+g\mu_BH_A(T),\tag{3.8}$$

and

$$\mathcal{H}_{1d}=-(2N)^{-1}\sum_{\mathbf{k}\mathbf{k}',ss'}\{J_Tz_T[1-(-1)^s|\gamma_{(T)\mathbf{k}}|]\times[1-(-1)^{s'}|\gamma_{(T)\mathbf{k}'}|]+J_Lz_L[1-\gamma_{(L)\mathbf{k}}]\times[1-\gamma_{(L)\mathbf{k}'}]\}n_{\mathbf{k}s}n_{\mathbf{k}'s'},\tag{3.9}$$

where $\mathbf{k}$ is the wave number and $s(=1,2)$ is the branch index. We have also used the definitions

$$\gamma_{(T)\mathbf{k}p}=z_T^{-1}\sum_m\exp[-i\mathbf{k}_T\cdot\mathbf{r}_m],\quad \gamma_{(L)\mathbf{k}}=z_L^{-1}\sum_n\exp[-i\mathbf{k}_L\cdot\mathbf{r}_n],\tag{3.10}$$

and

$$|\gamma_{(T)\mathbf{k}}|=[\gamma_{(T)\mathbf{k}p}\gamma_{(T)-\mathbf{k}p}]^{1/2},\tag{3.11}$$

where $\mathbf{r}_m$ and $\mathbf{r}_n$ denote vectors connecting a given Cr^{3+} lattice point on sublattice p to its nearest neighbors within the layer and in the two adjacent layers, respectively. The modification of the spin-wave energies $\omega_{\mathbf{k}s}$ by the diagonal perturbation $\mathcal{H}_{1d}$ can be treated by a renormalization process which makes use of the approximation[9,25]

$$n_{\mathbf{k}s}n_{\mathbf{k}'s'}=2n_{\mathbf{k}s}\langle n_{\mathbf{k}'s'}\rangle.\tag{3.12}$$

Combining (3.8), (3.9), and (3.12) yields an expression for the total energy

$$E=E_0+\sum_{\mathbf{k},s}\epsilon_{\mathbf{k}s}n_{\mathbf{k}s},\tag{3.13}$$

in terms of the renormalized spin-wave energies

$$\epsilon_{\mathbf{k}s}=2J_Tz_TS\xi_T[1-(-1)^s|\gamma_{(T)\mathbf{k}}|]+2J_Lz_LS\xi_L[1-\gamma_{(L)\mathbf{k}}]+g\mu_BH_A(T).\tag{3.14}$$

The renormalization coefficients, ξ_T and ξ_L, are independent of $\mathbf{k}$ and s, and are given by

$$\xi_T=1-(2SN)^{-1}\sum_{\mathbf{k},s}\langle n_{\mathbf{k}s}\rangle[1-(-1)^s|\gamma_{(T)\mathbf{k}}|],\tag{3.15}$$

$$\xi_L=1-(2SN)^{-1}\sum_{\mathbf{k},s}\langle n_{\mathbf{k}s}\rangle[1-\gamma_{(L)\mathbf{k}}].\tag{3.16}$$

The thermal averages are

$$\langle n_{\mathbf{k}s}\rangle=[\exp(\epsilon_{\mathbf{k}s}/k_BT)-1]^{-1},\tag{3.17}$$

since the excitations are still bosons. A calculation of the temperature dependence of the sublattice magnetization

$$M(T)=M(0)[1-(2NS)^{-1}\sum_{\mathbf{k},s}\langle n_{\mathbf{k}s}\rangle]\tag{3.18}$$

thus requires a solution of (3.15), (3.16), and (3.17) for ξ_T and ξ_L.

An iterative technique for obtaining the above solution has been discussed previously.[9] The present calculations were performed on a CDC-3600 digital computer. The summations were replaced by integrations over the first Brillouin zone of the reciprocal lattice appropriate for the lattice model of Fig. 2. The temperature dependence of $H_A(T)$ was assumed to obey the relation

$$H_A(T)=H_A(0)[M(T)/M(0)]^2,\tag{3.19}$$

in which the relative sublattice magnetization was taken from our NMR measurements. The $[M(T)]^2$ dependence in (3.19) is the spin-wave prediction[26] for single-ion anisotropies of the quadratic form. We have compared this prediction with Dillon's measured values[18] for $CrBr_3$ over the temperature range of our previous

[21] S. V. Maleev, Zh. Eksperim. i Teor. Fiz. **33**, 1010 (1957) [English transl.: Soviet Phys.—JETP **6**, 776 (1958)].
[22] T. Oguchi, Progr. Theoret. Phys. (Kyoto) **25**, 721 (1961).
[23] R. A. Tahir-Kheli and D. terHaar, Phys. Rev. **127**, 95 (1962).
[24] F. Keffer and R. Loudon, J. Appl. Phys., Suppl., **32**, 2S (1961).
[25] M. Bloch, Phys. Rev. Letters **9**, 286 (1962).
[26] J. Kanamori, *Magnetism* (Academic Press Inc., New York, 1963), Vol. 1, Chap. 4.

TABLE I. Summary of renormalized spin-wave fit for ferromagnetic CrI_3 in zero external field. The calculated values are based on $J_T/k_B=13.5°K$, $J_L/k_B=1.72°K$, $H_A(0)=28.6$ kOe, $g=2.07$, and $\nu(0)=49.393$ Mc/sec. The experimental frequencies correspond to the $\frac{1}{2}\leftrightarrow-\frac{1}{2}$ ^{53}Cr domain NMR.

T(°K)	ν_{obs} (Mc/sec)	ν_{calc} (Mc/sec)	$\nu_{calc}-\nu_{obs}$ (kc/sec)	ξ_T	ξ_L
1.65	49.392	49.390	−2	1.0000	1.0000
2.03	49.385	49.387	2	1.0000	1.0000
3.00	49.365	49.370	5	1.0000	1.0000
4.02	49.335	49.340	5	1.0000	1.0000
13.76	48.393	48.400	7	0.9981	0.9890
14.88	48.223	48.224	1	0.9975	0.9866
15.93	48.044	48.047	3	0.9970	0.9842
16.91	47.869	47.872	3	0.9963	0.9817
17.92	47.686	47.683	−3	0.9957	0.9789
19.05	47.473	47.460	−13	0.9948	0.9757
19.69	47.345	47.328	−17	0.9943	0.9737
24.95	46.093	46.101	8	0.9888	0.9550
25.25	46.010	46.024	14	0.9885	0.9538
26.23	45.747	45.765	18	0.9872	0.9498
26.71	45.612	45.636	24	0.9865	0.9478
27.43	45.418	45.438	20	0.9855	0.9447

$CrBr_3$ measurements.[9] The agreement was found to be excellent.

Using $H_A(0)=28.6$ kOe, $g=2.07$,[12] and $S=\frac{3}{2}$ a good fit of the renormalized theory to our ^{53}Cr data is obtained for

$$\begin{aligned} J_T/k_B &= 13.5\pm0.5°\text{K}\,, \\ J_L/k_B &= 1.72\mp0.20°\text{K}\,, \\ \nu(0) &= 49.393\pm0.005 \text{ Mc/sec}\,. \end{aligned} \tag{3.20}$$

A comparison of calculated and observed frequencies is given in Table I, which also lists the calculated renormalization constants. It is apparent that the intralayer interaction in CrI_3 is considerably larger than the interlayer interaction. However, the ratio $J_Tz_T/J_Lz_L=12$ is smaller than the corresponding ratio in $CrBr_3$.

B. Domain-Wall Magnetization

The sublattice magnetization in the walls is expected to decrease faster with increasing temperature than the domain magnetization.[27,28] The principal reason for this behavior is found in the thermal excitation of wall translations. Winter[28] has obtained an expression for the difference between domain and wall magnetizations for a cubic ferromagnet characterized by a single exchange constant and a uniaxial anisotropy. In our notation the expression is

$$M(T)_{\text{domain}}-M(T)_{\text{wall}}=(D/J)^{1/2} \times(k_BT/32\pi JS)\ln(D/D')\,, \tag{3.21}$$

where D' is a wall-stiffness parameter. This expression is valid if $k_BT\gg D$ and $k_BT\ll 2JS$. The linear dependence of (3.21) on T simply follows from the two-dimensional structure of the wall, i.e., the wave vector has no component normal to the wall for any wall excitation. It is tempting to use (3.21) to explain the linear temperature dependence of $\nu(T)_{\text{domain}}-\nu(T)_{\text{wall}}$ in CrI_3 and $CrBr_3$. However, a direct comparison of (3.21) with (2.1), (2.2) is not justified. Because of the plate-like crystal habit of these compounds it is expected that most of the domains are separated by 180° walls containing the c axis. Thus, the amplitude of thermal wall motions depends on both J_L and J_T. However, the largest average occupation numbers will be found for walls modes with $k_T<k_L$ since $J_L\ll J_T$. The average reduction of the wall magnetization due to thermally driven wall motions should therefore exhibit a temperature dependence intermediate to those of a linear structure ($M\propto T^{1/2}$) and a planar structure ($M\propto T$). The agreement between observed and calculated temperature exponents must therefore be fortuitous. Qualitatively, however, the experimental observations can be explained by noting that the effective exponent of T will be increased by the anisotropy at very low temperatures and by the interaction between wall excitations at higher temperatures. Furthermore, the small difference between the temperature coefficients of CrI_3(2.1) and $CrBr_3$(2.2) is related to the fact that both the anisotropy and average exchange energy increase in going from the bromide to the iodide.

The origin of the 0°K difference between the domain and domain wall ^{53}Cr frequencies is not entirely clear.[17] This difference corresponds to $\Delta H=-3.4$ kOe in CrI_3 and $\Delta H=-4.45$ kOe in $CrBr_3$. About half of the difference in each case (−1.95 and −2.43 kOe, respectively) can be accounted for by differences between the dipole field in the domains and at the center of the walls. Gossard *et al.*[17] have suggested that an anisotropic orbital hyperfine interaction might account for some of the discrepancy in $CrBr_3$. The orbital hyperfine anisotropy can be related to the anisotropy constant appearing in the spin Hamiltonian by the following second-order expression[29]

$$\Delta H_{hf}(\text{orb.})=-4DS\mu_B\langle r^{-3}\rangle/\lambda\,, \tag{3.22}$$

where $\langle r^{-3}\rangle$ is the appropriate expectation value of r^{-3}, and λ is the spin-orbit coupling constant. The negative sign in (3.22) is consistent with our definition of D (3.1). Using $\langle r^{-3}\rangle=21\times10^{24}$ cm^{-3}, $\lambda=87$ cm^{-1}, and $D=0.921$ cm^{-1} and 0.213 cm^{-1} for CrI_3 and $CrBr_3$, respectively, we find

$$\begin{aligned} CrI_3:&\quad \Delta H_{hf}(\text{orb})=-1.04\text{ kOe}\,, \\ CrBr_3:&\quad \Delta H_{hf}(\text{orb})=-0.24\text{ kOe}\,. \end{aligned} \tag{3.23}$$

Combining the calculated dipolar and orbital hyperfine anisotropies we find differences of −0.4 kOe and −1.8 kOe in CrI_3 and $CrBr_3$, respectively, which remain unaccounted for. Although the agreement in the case of CrI_3 is very good, the above analysis should be viewed with some caution. In the first place, the wall dipole-

[27] H. Suhl, Bull. Am. Phys. Soc. **5**, 175 (1960).
[28] J. M. Winter, Phys. Rev. **124**, 452 (1961).
[29] A. Abragam and M. H. L. Pryce, Proc. Roy. Soc. (London) **A205**, 135 (1951).

field estimates are based on the assumption that $H_{\rm dip}(\text{wall}) = -\frac{1}{2}H_{\rm dip}(\text{domain})$, and hence ignore the details of the wall structure. Because the walls in $CrBr_3$ and CrI_3 are quite narrow, the magnitude of the dipole field near the center of the wall presumably exceeds this estimate in both compounds. Thus, the dipolar anisotropies given above probably underestimate the true difference between the domain and domain wall dipole fields. Secondly, the single-ion anisotropy term in (3.1) is not consistent with the positive g-shifts observed by Dillon. For this reason, the validity of (3.22) is somewhat in doubt. In this connection it is significant that in $CrCl_3$ a hyperfine anisotropy of -1.0 kOe has been measured directly[8] by comparing the ^{53}Cr NMR frequencies for sublattice magnetization directions parallel and perpendicular to the c axis, taking account of dipolar effects as above. Since $CrCl_3$ is the most ionic member of this series, orbital effects must be quite small in this case.

IV. CALCULATION OF THE CURIE TEMPERATURE

To this point, the exchange constants which we have obtained for the anhydrous chromium (III) halides have not been subjected to an independent quantitative test. For this reason we have carried out a random-phase (RPA) Green-function calculation of the Curie temperatures of CrI_3 and $CrBr_3$, based on the exchange constants deduced from the low-temperature renormalized spin-wave analyses.

In the following we make use of the double-time temperature-dependent Green function formalism. This technique has been reviewed in detail by Zubarev[30] and applied to isotropic ferromagnets by Tahir-Kheli and terHaar,[31] and others.[32] We require the following two properties of retarded Green's functions.

Relation (1):

$$E\langle\langle A;B\rangle\rangle_E = (2\pi)^{-1}\langle[A,B]\rangle + \langle\langle[A,\mathcal{H}];B\rangle\rangle_E. \quad (4.1)$$

This expression is the equation of motion of the Fourier transform $\langle\langle A;B\rangle\rangle_E$ of the Green's function $\langle\langle A(t);B(t')\rangle\rangle$, involving the Heisenberg operators $A(t)$ and $B(t')$. We follow the usual practice of denoting Green's functions by double-pointed brackets and correlation functions by single-pointed brackets.

Relation (2):

$$\langle B(t')A(t)\rangle = \lim_{\epsilon\to+0} i\int_{-\infty}^{+\infty} \frac{\langle\langle A;B\rangle\rangle_{E=\omega+i\epsilon} - \langle\langle A;B\rangle\rangle_{E=\omega-i\epsilon}}{\exp(\omega/k_BT)-1} \times\exp[-i\omega(t-t')]d\omega. \quad (4.2)$$

This expression relates the correlation function of the operators $A(t)$ and $B(t')$ to the corresponding Green's function.

We now evaluate the Green's function $\langle\langle S_\alpha^+;B_\delta\rangle\rangle_E$ from its equation of motion. The operators S_α^+ and B_δ refer to lattice positions α and δ. The single Greek subscripts thus combine the cell and sublattice designations, i.e., $\alpha\equiv i,p$. The relevant commutation relations are given by (we use a system of units in which $\hbar=1$)

$$\begin{aligned}[S_\alpha^+,S_\delta^-] &= 2\delta_{\alpha\delta}S_\alpha^z,\\ [S_\alpha^+,S_\delta^z] &= -\delta_{\alpha\delta}S_\alpha^+.\end{aligned} \quad (4.3)$$

We use the Hamiltonian (3.1) and find

$$\begin{aligned}E\langle\langle S_\alpha^+;B_\delta\rangle\rangle_E &= (2\pi)^{-1}\langle[S_\alpha^+,B_\delta]\rangle\\ &+2J_T\textstyle\sum_\beta\{\langle\langle S_\beta^zS_\alpha^+;B_\delta\rangle\rangle_E - \langle\langle S_\alpha^zS_\beta^+;B_\delta\rangle\rangle_E\}\\ &+2J_L\textstyle\sum_\gamma\{\langle\langle S_\gamma^zS_\alpha^+;B_\delta\rangle\rangle_E - \langle\langle S_\alpha^zS_\gamma^+;B_\delta\rangle\rangle_E\}\\ &+D\langle\langle(S_\alpha^+S_\alpha^z+S_\alpha^zS_\alpha^+);B_\delta\rangle\rangle_E.\end{aligned} \quad (4.4)$$

The sums in (4.4) over the β and γ lattice points are restricted to the z_T and z_L neighbors which are exchange coupled to the α lattice point by J_T and J_L, respectively. We now employ the random-phase approximation (RPA)[33] to decouple the higher-order Green's functions which appear in (4.4). We take

$$\langle\langle S_\alpha^zS_\beta^+;B_\delta\rangle\rangle_E = \langle S_\alpha^z\rangle\langle\langle S_\beta^+;B_\delta\rangle\rangle_E, \quad (\alpha\neq\beta) \quad (4.5)$$

and[34]

$$\langle\langle(S_\alpha^+S_\alpha^z+S_\alpha^zS_\alpha^+);B_\delta\rangle\rangle_E = 2\langle S_\alpha^z\rangle\langle\langle S_\alpha^+;B_\delta\rangle\rangle_E. \quad (4.6)$$

The decoupling scheme (4.6) for Green's functions arising from the single-ion anisotropy is equivalent to replacing $(S^z)^2$ by $2\langle S^z\rangle S^z$ in the Hamiltonian (3.1). Thus (4.6) corresponds to a molecular field approximation. This approximation is adequate if $D\ll k_BT_C$, a condition which is well satisfied in CrI_3 and $CrBr_3$. Since all lattice points in CrI_3 are magnetically equivalent, (4.4) can be written in its decoupled form as

$$\begin{aligned}(E-\mathcal{E})\langle\langle S_\alpha^+;B_\delta\rangle\rangle_E &= \delta_{\alpha\delta}(2\pi)^{-1}\langle[S_\alpha^+,B_\delta]\rangle\\ &-2J_T\langle S_\alpha^z\rangle\textstyle\sum_\beta\langle\langle S_\beta^+;B_\delta\rangle\rangle_E\\ &-2J_L\langle S_\alpha^z\rangle\textstyle\sum_\gamma\langle\langle S_\gamma^+;B_\delta\rangle\rangle_E,\end{aligned} \quad (4.7)$$

where

$$\mathcal{E} = 2\langle S^z\rangle(J_Tz_T+J_Lz_L+D). \quad (4.8)$$

We proceed by introducing a spatial Fourier transformation to reciprocal lattice coordinates of the following form

$$\langle\langle S_{ip}^+;B_{i'p'}\rangle\rangle_E = N^{-1}\textstyle\sum_{\mathbf{k}} G_{\mathbf{k}(p,p')} \times\exp[i\mathbf{k}\cdot(\mathbf{r}_{ip}-\mathbf{r}_{i'p'})] \quad (4.9)$$

$$G_{\mathbf{k}(p,p')} = \textstyle\sum_{i'}\langle\langle S_{ip}^+;B_{i'p'}\rangle\rangle_E \times\exp[-i\mathbf{k}\cdot(\mathbf{r}_{ip}-\mathbf{r}_{i'p'})], \quad (4.10)$$

[30] D. N. Zubarev, Usp. Fiz. Nauk **71**, 71 (1960) [English transl.: Soviet Phys.—Usp. **3**, 320 (1960)].
[31] R. A. Tahir-Kheli and D. terHaar, Phys. Rev. **127**, 88 (1962); **127**, 95 (1962).
[32] For other references see, for example, A. C. Hewson and D. terHaar, Physica **30**, 271 (1964).
[33] S. V. Tyablikov, Ukr. Mat. Zh. **11**, 287 (1959).
[34] F. B. Anderson and H. B. Callen, Phys. Rev. **136**, A1068 (1964).

where the sums on $\mathbf{k}$ and i' span the N points which belong to the same branch (s) and sublattice (p'), respectively. Applying (4.7) and (4.9) to (4.10) we find a relation between Green functions coupling different sublattices:

$$(E-\mathcal{E})G_{\mathbf{k}(p,p')}=\delta_{pp'}(2\pi)^{-1}\langle[S_{ip}{}^{+};B_{ip}]\rangle-\langle S^{z}\rangle\{2J_{T}z_{T}\gamma_{(T)\mathbf{k}p}{}^{*}G_{\mathbf{k}(3-p,p')}+2J_{L}z_{L}\gamma_{(L)\mathbf{k}}G_{\mathbf{k}(p,p')}\}\,. \qquad (4.11)$$

By solving two simultaneous equations for $G_{\mathbf{k}(1,1)}$ and $G_{\mathbf{k}(2,1)}$ using (4.11) we obtain

$$4\pi G_{k(1,1)}=\sum_{s=1,2}\left[\frac{\langle[S_{i1}{}^{+},B_{i1}]\rangle}{E-\langle S^{z}\rangle\{2J_{T}z_{T}(1-(-1)^{s}|\gamma_{(T)\mathbf{k}}|)+2J_{L}z_{L}(1-\gamma_{(L)\mathbf{k}})+2D\}}\right]. \qquad (4.12)$$

The correlation function $\langle B(t)S^{+}(t)\rangle$ can now be evaluated from (4.2), (4.9) and (4.12). The result is

$$\langle B_{ip}S_{ip}{}^{+}\rangle=(2N)^{-1}\langle[S_{ip}{}^{+},B_{ip}]\rangle \times\textstyle\sum_{\mathbf{k},s}[\exp(F_{\mathbf{k}s}\langle S^{z}\rangle/k_{B}T)-1]^{-1}, \qquad (4.13)$$

where

$$F_{\mathbf{k}s}=\{2J_{T}z_{T}(1-(-1)^{s}|\gamma_{(T)\mathbf{k}}|) +2J_{L}z_{L}(1-\gamma_{(L)\mathbf{k}})+2D\}\,. \qquad (4.14)$$

The energies $F_{\mathbf{k}s}\langle S^{z}\rangle$ are very similar to the renormalized spin-wave energies (3.14). The difference lies in the fact that the renormalization in the random-phase approximation is proportional to the magnetization and not the average energy.

We can now estimate the Curie temperature. We let $B=S^{-}$ and carry out a linear expansion of the exponentials. The latter is justified by the fact that $F_{\mathbf{k}s}\langle S^{z}\rangle \ll k_{B}T$ near T_C. Hence,

$$\langle S(S+1)-S^{z}-(S^{z})^{2}\rangle=k_{B}TN^{-1}\textstyle\sum_{\mathbf{k},s}(F_{\mathbf{k}s})^{-1}. \qquad (4.15)$$

As the limit $T\rightarrow T_C$ is approached from below, $\langle S^{z}\rangle\rightarrow 0$ and $\langle(S^{z})^{2}\rangle\rightarrow\frac{1}{3}S(S+1)$. The limiting value of $\langle(S^{z})^{2}\rangle$ follows from the decoupling scheme (4.6) which causes the effect of $D(S^{z})^{2}$ on the energy to vanish at T_C. Thus we obtain the RPA Green's-function prediction

$$k_{B}T_{C}(\mathrm{RPA})=\tfrac{2}{3}S(S+1)N[\textstyle\sum_{\mathbf{k},s}(F_{\mathbf{k}s})^{-1}]^{-1}, \qquad (4.16)$$

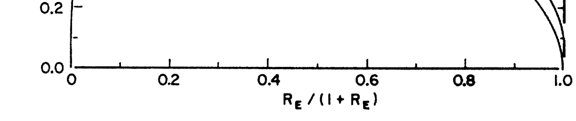

FIG. 3. Plot of Curie temperatures for the magnetic structure of Fig. 2 as a function of $R_E=J_Lz_L/J_Tz_T$ for three values of $2D/J_Tz_T$. The ratio T_C(RPA)/T_C(MF) denotes the random-phase Green's-function prediction relative to the molecular field result. The spin-wave values of $R_E/(1+R_E)$ for $CrBr_3$ and CrI_3 are indicated in the upper left-hand corner. The respective values of $2D/J_Tz_T$ are 0.0247 and 0.0654.

which compares with the molecular-field prediction

$$k_{B}T_{C}(\mathrm{MF})=\tfrac{2}{3}S(S+1)(J_{T}z_{T}+J_{L}z_{L})\,. \qquad (4.17)$$

We have calculated T_C for $CrBr_3$ and CrI_3 from (4.16) on the basis of the spin-wave exchange constants (Table IV) and anisotropies and g values obtained by Dillon[12,18] from ferromagnetic resonance studies. The sum over the $2N$ reciprocal lattice points was evaluated by means of a numerical integration over the same Brillouin zone used in the spin-wave calculations. The results are compared in Table II with the molecular-field (MF) and experimental Curie temperatures. The random phase Green's function ordering temperatures are seen to be in excellent agreement with the experimental temperatures. The molecular-field predictions, on the other hand are much too high.

The general dependence of T_C on J_T, J_L, and D is shown in Fig. 3, which gives the calculated ratio T_C(RPA)/T_C(MF) as a function of $R_E/(1+R_E)$, where $R_E=J_Lz_L/J_Tz_T$, for several values of $R_A(=2D/J_Tz_T)$. The calculated curves demonstrate the strong dependence of T_C(RPA) on the ratio J_L/J_T. For zero anisotropy, T_C(RPA)$=0$ for either the one-dimensional ($J_T=0$) or two-dimensional ($J_L=0$) systems, in agreement with the predictions[35] of spin-wave theory. The highest ordering temperature, for any value of the anisotropy is predicted for $J_Lz_L/J_Tz_T=\frac{1}{2}$, i.e., when the average exchange interaction has the same magnitude in any crystal direction. For this ratio of exchange constants and $R_A=0$ we calculate T_C(RPA)/T_C(MF) $=0.588$. This value compares with T_C(RPA)/T_C(MF) $=0.659$ obtained by Tahir-Kheli and terHaar[31] for the simple-cubic lattice. Our lower value is a consequence of the smaller coordination number (five compared to six) of our lattice.

TABLE II. Comparison of observed and calculated Curie temperatures for $CrBr_3$ ($J_T/k_B=8.25$°K, $J_L/k_B=0.497$°K, $D/k_B=0.306$°K) and CrI_3 ($J_T/k_B=13.5$°K, $J_L/k_B=1.72$°K, $D/k_B=1.325$°K). The random-phase Green's-function and molecular-field results are denoted by T_C(RPA) and T_C(MF), respectively.

	T_C(obs)	T_C(RPA)	T_C(MF)
$CrBr_3$	32.5[a]	33.6	64.3
CrI_3	68[b]	68.2	109.8

[a] Reference 7. [b] Reference 12.

[35] J. VanKranendonk and J. H. Van Vleck, Rev. Mod. Phys. **30**, 1 (1958).

V. SUMMARY AND DISCUSSION

The results of the present work can be grouped into two principal categories. The first concerns the magnetic and electric hyperfine coupling constants of ^{53}Cr in CrI_3. The second concerns the temperature dependence of the sublattice magnetization, and the magnitudes of the intralayer and interlayer exchange constants derived from it.

The ^{53}Cr magnetic hyperfine field ($H_{hf}\|c$) and quadrupole coupling constant in CrI_3 are compared in Table III with the corresponding values in $CrBr_3$ and $CrCl_3$. The hyperfine fields were obtained from the extrapolated 0°K zero-field ^{53}Cr frequencies corrected for dipolar effects. The dipole fields (H_d) were estimated (from point dipole sums) to be -0.65, -0.81, and $+2.24$ kOe for the iodide, bromide, and chloride, respectively. Since the net hyperfine field (H_{hf}) is negative[8,16] in these compounds, H_d has the same sign as H_{hf} in CrI_3 and $CrBr_3$ and the opposite sign in $CrCl_3$. The dipole field in $CrCl_3$ is positive because the spins are ordered perpendicular to the c axis. For this reason the parallel hyperfine field for $CrCl_3$ given in Table III also includes a -1.0 kOe correction for the measured[8] hyperfine anisotropy. An inspection of Table III reveals a monotonic decrease in H_{hf} with increasing size of the ligand. The reduction is particularly large for CrI_3.

It is possible to estimate the spin and orbital contributions to the observed hyperfine fields. The orbital hyperfine field is given by

$$H_{hf}(\mathrm{orb})=2S\mu_B\langle r^{-3}\rangle(g-2.0023). \tag{5.1}$$

Using $\langle r^{-3}\rangle=21\times10^{24}$ cm^{-3} as in Sec. III and $g=2.07$ and 2.007 for CrI_3 and $CrBr_3$,[12,18] we find

$$\begin{aligned} CrI_3:&\quad H_{hf}(\mathrm{orb})=+41\pm6\ \mathrm{kOe}, \\ CrBr_3:&\quad H_{hf}(\mathrm{orb})=+2.7\pm0.5\ \mathrm{kOe}. \end{aligned} \tag{5.2}$$

The error limits in (5.2) reflect the uncertainties in the g values, but do not include possible errors in the $\langle r^{-3}\rangle$ estimate. The latter may be in error by as much as 20%. The orbital hyperfine field in $CrCl_3$ is presumably less than 1 kOe. The spin hyperfine fields are therefore

$$\begin{aligned} CrI_3:&\quad H_{hf}(\mathrm{spin})=-245\pm6\ \mathrm{kOe}, \\ CrBr_3:&\quad H_{hf}(\mathrm{spin})=-243\pm1\ \mathrm{kOe}, \\ CrCl_3:&\quad H_{hf}(\mathrm{spin})=-266\pm1\ \mathrm{kOe}. \end{aligned} \tag{5.3}$$

It is interesting to note that the large difference between the ^{53}Cr hyperfine fields in CrI_3 and $CrBr_3$ can be explained entirely on the basis of a difference in the orbital hyperfine interaction.

The quadrupole coupling constants are not a monotonic function of ligand size. The largest contribution to the electric field gradient, on the basis of the ionic-point-charge model, arises from the Cr^{3+} ions. This contribution decreases with increasing ligand size because of the resulting lattice expansion. It is likely that the explanation for the anomalously large CrI_3 coupling constant lies in a relatively large contribution from the distorted octahedral arrangement of I^- ions surrounding each Cr^{3+} ion.

TABLE III. Summary of ^{53}Cr magnetic hyperfine fields parallel to the c axis and quadrupole coupling constants in CrX_3(X=Cl, Br, I).

	H_{hf}(kOe)	$h^{-1}e^2qQ$ (Mc/sec)
$CrCl_3$[a]	266.4	0.880
$CrBr_3$[b]	240.6	0.592
CrI_3	204.6	0.744

[a] Reference 8. [b] Reference 16.

The observation of the ^{53}Cr NMR in both domains and domain walls confirms that CrI_3 has a spontaneous magnetic moment below T_C and thus justifies the assumption that $J_L>0$. The domain and wall assignments are based on the observed linewidths, intensities, and temperature dependences, as well as the general similarity of the ^{53}Cr resonance spectrum in CrI_3 to that observed[17] in ferromagnetic $CrBr_3$. In both compounds the large difference between the domain and wall magnetizations at nonzero temperatures is a direct consequence of the small interlayer exchange energy relative to k_BT_C and $g\mu_BH_A$ (i.e., $J_L<J_T$, $J_L\sim g\mu_BH_A$).

The temperature dependence of the domain sublattice magnetization of CrI_3 follows the predictions of a renormalized parametric spin-wave model with a suitable choice of exchange constants. A fit of the theory to our experimental data clearly demonstrates that $J_L<J_T$ as in the case of $CrCl_3$ and $CrBr_3$. The magnitudes of J_Tz_T and J_Lz_L for the three compounds are listed in Table IV. In order to provide an independent test for the validity of the low-temperature spin-wave calculations we have carried out a random-phase Green-function calculation of T_C for the ferromagnets $CrBr_3$ and CrI_3. The close agreement between calculated and observed ordering temperatures is quite gratifying, particularly since these calculations did not involve any adjustable parameters. Unfortunately, no precise information exists concerning the accuracy of the RPA Green's-function method when applied to the calculation of T_C for anisotropic ferromagnets. The extent to

TABLE IV. Summary of exchange constants for antiferromagnetic $CrCl_3$ and ferromagnetic $CrBr_3$ and CrI_3, based on renormalized spin-wave analyses of low-temperature sublattice magnetization data.

	J_Tz_T/k_B(°K)	J_Lz_L/k_B(°K)	$\lvert J_Tz_T/J_Lz_L\rvert$
$CrCl_3$[a]	15.75	-0.037	426
$CrBr_3$[b]	24.75	0.99	25
CrI_3	40.5	3.44	12

[a] Reference 8. [b] Reference 9.

which the exchange and anisotropy parameters may be affected by thermal expansion is also not known in the present case. For these reasons it is not possible to use the agreement between calculated and observed values of T_C to obtain a quantitative estimate of the accuracy of J_T and J_L. The molecular-field predictions of T_C were shown to be quite inaccurate. The errors which are introduced by the molecular field model are much more serious in the CrX_3 compounds than is usually the case. This failure is due to the low coordination number of our lattice, and the inherent instability of the two-dimensional ferromagnet. Thus, when J_L/J_T is small, the neglect of structure effects by the molecular field model is no longer justified. The RPA Green's-function technique, on the other hand, gives good agreement with the observed Curie temperature when coupled with spin-wave exchange parameters obtained from the low-temperature sublattice magnetization behavior. The most important result of this investigation, therefore, lies in the demonstration that the sublattice magnetization behavior of the relatively complex ferromagnets CrI_3 and $CrBr_3$ can be accounted for in a self-consistent way by an appropriate renormalized spin-wave theory at low temperatures and by the random-phase approximation at T_C. It would be interesting to compare the two methods at intermediate temperatures provided that sublattice magnetization data for CrI_3 or $CrBr_3$ become available for this range.

Finally, we may compare the experimental values which have been reported for the paramagnetic Curie temperature (θ) with those predicted by the molecular field model using our exchange constants. For the magnetic structure appropriate for CrI_3 and $CrBr_3$ the molecular field model gives $\theta = T_C$. Hence, we may compare directly the last column of Table II with the experimental values of $+70°K$ for CrI_3 and $+51°K$ for $CrBr_3$ derived from high-temperature ($T \lesssim 400°K$) magnetic susceptibility measurements.[10] The agreement is seen to be very poor, particularly for CrI_3 where the calculated value is 57% higher than the observed one. This lack of agreement is not surprising in view of the practical difficulty of attaining the high-temperature limit in measurements of the susceptibility. Because of the large ratio of θ/T_C encountered in the CrX_3 compounds it is unlikely that the experimental χ^{-1}-versus-T plots yield accurate estimates of the Curie-Weiss asymptotes at temperatures below $\sim 400°K$.

ACKNOWLEDGMENTS

The author wishes to express his thanks to Dr. C. E. Olson and J. E. Hesse for supplying the CrI_3 samples used in this study. The author is also indebted to D. C. Barham for carrying out many of the resonance experiments. Helpful discussions with Dr. D. C. Wallace, Dr. E. D. Jones, and Dr. A. C. Gossard are gratefully acknowledged.